Chemical Science

ROYAL SOCIETY OF CHEMISTRY

EDGE ARTICLE

View Article Online
View Journal | View Issue

Cite this: *Chem. Sci.*, 2024, **15**, 3148

All publication charges for this article have been paid for by the Royal Society of Chemistry

Stereo effects for efficient synthesis of orange-red multiple resonance emitters centered on a pyridine ring†

Mingxu Du,[ab] Minqiang Mai,[a] Dongdong Zhang,[ab] Lian Duan [ab] and Yuewei Zhang *[bc]

Received 3rd December 2023
Accepted 16th January 2024

DOI: 10.1039/d3sc06470k

rsc.li/chemical-science

Despite theoretical difficulties, we herein demonstrate an effective strategy for the inaugural synthesis of an orange-red multiple resonance (MR) emitter centered on a pyridine ring *via* stereo effects. Compared to conventional benzene-centered materials, the pyridine moiety in the novel MR material acts as a co-acceptor. This results in a significant spectral redshift and a narrower spectrum, as well as an improved photoluminescence quantum yield (PLQY) due to the formation of intramolecular hydrogen bonds. As envisioned, the proof-of-concept emitter Py-Cz-BN exhibits bright orange-red emission peaking at 586 nm with a small full width at half maximum (FWHM) of 0.14 eV (40 nm), exceeding both the wavelength and FWHM achieved with benzene-centered BBCz-Y. Benefiting from high PLQYs (>92%) and suppressed chromophore interactions, the optimized organic light-emitting diodes achieved high maximum external quantum efficiencies of 25.3–29.6%, identical small FWHMs of 0.18 eV (54 nm), and long lifetimes over a wide range of dopant concentrations (1–15 wt%). The performance described above demonstrates the effectiveness of this molecular design and synthesis strategy in constructing high performance long-wavelength MR emitters.

Introduction

Narrowband emissive organic emitters that can harvest triplet excitons for emission are highly desired for the next generation of cost-effective, energy-saving, and wide color gamut ultra-high-definition organic light-emitting diode (OLED) displays.[1] However, commercially available organic emitters are limited by the large structural displacements between the ground (S_0) and singlet excited (S_1) states, resulting in inherently broad emission spectra with full width at half maximum (FWHM) values exceeding 40 nm.[2] Although it is possible to obtain relatively narrower electroluminescence (EL) spectra by using color optical filters or microcavities, these methods inevitably result in energy losses and increased costs. Therefore, it is critical to develop molecular design and synthesis strategies for narrowband red (R)–green (G)–blue (B) dyes before OLEDs can become the ultimate display.

Hatakeyama *et al.* have recently developed a new type of organic light-emitting material known as multiple resonance thermally activated delayed fluorescence (MR-TADF), which was achieved by creating rigid boron-doped and nitrogen-doped polycyclic aromatic hydrocarbons (B,N-PAHs) to overcome the aforementioned limitations.[1b,3] A typical B,N type MR-TADF molecule can achieve a specific separation of the highest occupied (HOMO) and lowest unoccupied (LUMO) molecular orbitals at the atomic level. This enables a small singlet-triplet energy gap (ΔE_{st}) that triggers triplet-to-singlet upconversion and suppresses vibrational coupling and relaxation through the formation of specific non-bonding orbitals, resulting in narrowband emission. For instance, since the classical DABNA, several high-efficiency blue MR-TADF emitters have been reported. These emitters have enabled the realization of narrowband OLEDs with external quantum efficiencies (EQEs) that exceed 30% and small FWHMs below 20 nm (<0.10 eV).[1b,4] Meanwhile, there is rapid development in green MR-TADF materials, with several systems capable of achieving CIEy values exceeding 0.70 under electroluminescence (EL) conditions.[3d,e,i,m,5] However, there are few examples of orange or red MR-TADF dyes compared to the aforementioned colours.[3j,5a,6] Therefore, it is urgent to continuously develop new MR-TADF skeletons and synthesis strategies before the new generation of wide color gamut materials and devices can be fully utilized.

Previous studies have demonstrated that the pyridine group can act as a co-acceptor (A) for efficient TADF materials. This can increase the strength of the acceptor, resulting in significant spectral redshifts. Additionally, the pyridine group can improve the chemical stability and structural rigidity of the

[a]*Key Lab of Organic Optoelectronics and Molecular Engineering of Ministry of Education, Department of Chemistry, Tsinghua University, Beijing 100084, P. R. China*
[b]*Laboratory of Flexible Electronics Technology, Tsinghua University, Beijing 100084, P. R. China. E-mail: zhangyuewei@mail.tsinghua.edu.cn*
[c]*Applied Mechanics Lab, School of Aerospace Engineering, Tsinghua University, Beijing 100084, P. R. China*

† Electronic supplementary information (ESI) available. CCDC 2297213. For ESI and crystallographic data in CIF or other electronic format see DOI: https://doi.org/10.1039/d3sc06470k

Fig. 1 Molecular design strategy for pyridine-centered MR-TADF emitters (Py-MR-TADF).

material by forming potential intramolecular hydrogen bonds. This, in turn, promotes high photoluminescence quantum yields (PLQYs) and narrow fluorescence bands.[7] Furthermore, our recent research has shown that the creation of *para*-B–π–A structures can improve the charge transfer (CT) properties of MR-TADF molecules, leading to emissions with a bathochromic shift.[6a,8] Therefore, introducing pyridinyl co-acceptors, particularly constructing new pyridine-centered skeletons (which have simple structures and low molecular weights), is an effective strategy for obtaining superior long-wavelength MR-TADF emitters (Fig. 1). However, direct synthesis of MR-TADF emitters centred on pyridine (Py-MR-TADF) is challenging due to the basicity of pyridine, which makes it susceptible to coordination with boron trihalides.

Although there were theoretical difficulties, we have successfully demonstrated an effective method for synthesising an orange-red Py-MR-TADF emitter through stereo effects. The Py-MR-TADF emitter has large-site resistive substituents which can prevent molecular aggregation. This, in addition to the previously mentioned benefits of spectral redshift and appropriate spectral narrowing, makes it a promising candidate for further research. As envisioned, the proof-of-concept emitter Py-Cz-BN shows a bright orange-red emission peaking at 586 nm with a small FWHM of 0.14 eV (40 nm), *i.e.*, not only does it achieve a significant redshift of more than 37 nm, but also a narrowing of the spectrum when compared to the benzene-centered BBCz-Y (emission maximum: 549 nm and FWHM: 0.17 eV/42 nm). Benefiting from the high PLQYs (>92%) and suppressed chromophore interactions, the optimized OLEDs simultaneously achieved high maximum external quantum efficiencies (EQE_{max}s) of 25.3–29.6% and identical small FWHMs of 0.18 eV (54 nm) over a wide range of dopant concentrations (1–15 wt%). Moreover, an impressively long LT90 (time to decay to 90% of the initial luminance) of 152 hours was recorded at an initial brightness of 5000 cd m^{-2}. The results above meet the high demand for orange-red emissive materials in automotive taillights, confirming the significant advantages of this molecular design strategy.

Results and discussion

Synthesis

As shown in Fig. 2a, similar to the conventional B–N type MR-TADF, the target molecule Py-Cz-BN was prepared in two steps

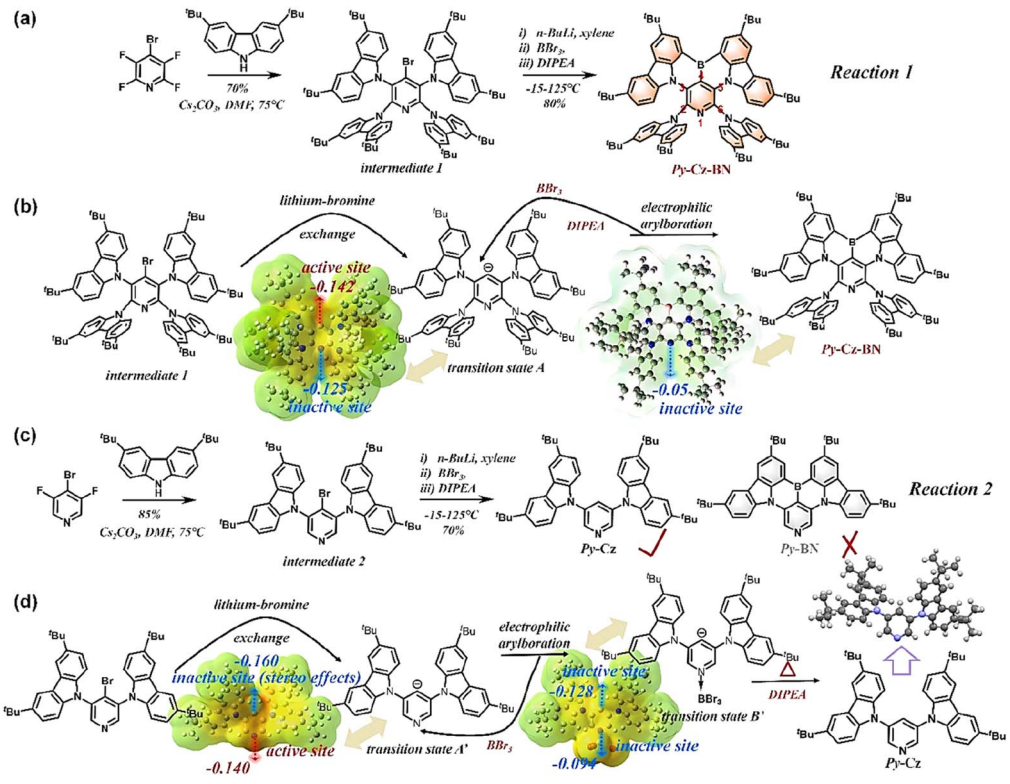

Fig. 2 (a) The synthetic procedures of Py-Cz-BN. (b) Possible reaction mechanism of Py-Cz-BN. (c) Our failure to synthesize Py-BN. (d) Possible reaction mechanism of Py-Cz. The ESP calculations of transition states were performed with the Gaussian 16 package, using the density functional theory (DFT) method with the B3LYP hybrid functional.

from a commercially available starting material, 4-bromo-2,3,5,6-tetrafluoropyridine. Expensive precious metal catalysts were not required, and intermediate 1 was easily synthesized with a good yield (70%) through an aromatic nucleophilic substitution reaction between 4-bromo-2,3,5,6-tetrafluoropyridine and 3,6-ditertbutyl carbazole (^{t}Cz). The Py-Cz-BN compound was synthesized in 80% yield by introducing a boron atom in one pot through a lithium–bromine exchange reaction with *n*-butyllithium, electrophilic trapping with boron tribromide, and tandem electrophilic arylboration in the presence of three equivalents of diisopropylethylamine. To our knowledge, 80% represents one of the highest yields achievable for a lithiation strategy,[9] indicating promising prospects for the commercialization of B–N based MR-TADF emitters. To demonstrate that the efficient synthesis of Py-Cz-BN stems from stereo effects, we here introduce the synthesis of Py-BN as a comparison. The nucleophilic aromatic substitution reaction was used to produce intermediate 2 with an 85% yield (Fig. 2c), following the same strategy. However, the desired Py-BN was not formed during the 'one-pot' lithiation–borylation reaction due to the absence of site-resistive substituents (^{t}Cz) at positions 2 and 6. Instead, only a dehalogenation by-product was produced (Fig. 2c, d and S5†). To clarify the mechanism of the above reactions, we calculated electrostatic potential (ESP) maps to evaluate the chelating ability of the possible intermediates. As demonstrated in Fig. 2b, d and S1–S4,† the electron-sharing pairs (ESPs) of the carbon anion and pyridine N in transition state A′ are 0.160 and 0.140, respectively. These values are both greater than those of transition state A (carbon anion: 0.142 and pyridine N: 0.125), indicating that the site resistive substituents can reduce the reactivity of the aforementioned sites. For reaction 2, transition state B′ is preferred over transition state A′ due to the stereo effects of boron tribromide coordinating with pyridine N, despite the higher ESP of the carbon anion in transition state A′ (Fig. 2d). Following the generation of transition state B′, the ESP of the carbon-negative ion is only 0.128. This value is no longer sufficient for subsequent electrophilic arylboration, resulting in the formation of only the debromination product for reaction 2. Similarly, in reaction 1, the introduction of site resistive substituents reduces the ESP value of pyridine N to 0.125. This reduction prevents pyridine N from coordinating with BBr3, resulting in the formation of only the target molecule Py-Cz-BN through electrophilic arylboration with the carbon anion (Fig. 2b). Upon obtaining Py-Cz-BN, the electrostatic potential of pyridine N is further reduced to 0.05, preventing any additional side-reactions and ensuring the effectiveness of the aforementioned design and synthesis strategy. Please refer to the ESI† for NMR, mass spectrometry, and elemental analysis of all newly synthesized materials.

Crystallography

The single crystal of Py-Cz-BN was grown by slow diffusion of methanol into its solution in dichloromethane (3 : 1, v/v). As shown in Fig. 3a and b, the molecular configuration changes significantly when the MR center varies from a phenyl (BBCz-Y)[3j] to a pyridinyl (Py-Cz-BN). BBCz-Y's BCz-BN core exhibits a boat-shaped conformation due to the large repulsive force generated by the ipsilateral site resistive substituents. However, Py-Cz-BN's BCz-BN core shows a planar structural feature because the two ^{t}Cz groups are located on both sides of the skeleton, effectively moderating the repulsive force problem faced by BBCz-Y. Previous studies have demonstrated that planar molecular structures are advantageous for achieving narrowband emissions,[10] whereas boat-shaped structures are not.[11] Therefore, replacing the phenyl core with a pyridine center can be an effective strategy for constructing high-performing MR-TADF emitters. In addition, the bilaterally shielded Py-Cz-BN is theoretically superior in suppressing concentration aggregation compared to the unilaterally clad BBCz-Y.[3c] As anticipated, the Py-Cz-BN crystal does not exhibit π–π stacking due to the loose arrangement of molecules along the *c* axis with a side-slipping stacking mode (the interlayer spacing increased up to 9.6 Å, Fig. 3c). In this case, intermolecular interactions are significantly suppressed, greatly reducing the effect of concentration on luminescence. Two intramolecular hydrogen bonds of CH···Ns, with a distance of about 2.5 Å, were found between the pyridine nitrogen atom and the proximal C–H bonds of the ^{t}Cz moieties (Fig. 3b).

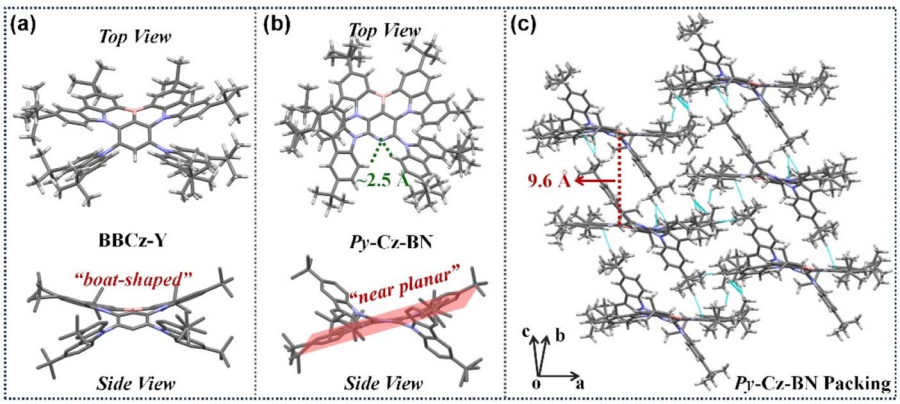

Fig. 3 (a) X-ray crystal structure of BBCz-Y (single crystal file taken from ref. [3j]). (b) X-ray crystal structure of Py-Cz-BN. (c) Packing mode of Py-Cz-BN.

These bonds limit the rotation between the donor and acceptor groups in the molecule, resulting in a narrower luminescence spectrum and an increased PLQY value.

Theoretical calculations

To verify the superiority of the above molecular design, we further performed density-functional theory (DFT) and time-dependent DFT (TD-DFT) calculations based on the single-crystal structure/optimized structure using the B3LYP/6-31G(d) method. As shown in Fig. 4a, Py-BN and BCz-BN exhibit almost identical HOMO/LUMO distributions and FWHM values (Py-BN: 0.09 eV/16 nm; BCz-BN: 0.09 eV/17 nm), which indicates that the central pyridine ring does not alter the intrinsic MR-TADF properties of the molecules. However, Py-BN shows a significant redshift in the emission spectrum, indicating its potential for constructing highly efficient long-wavelength MR-TADF emitters. As for Py-Cz-BN, the introduction of site-resistive substituents resulted in the expansion of the HOMO onto the peripheral donors, while the LUMO remained on the BCz-BN core (Fig. 4b). This unique distribution of frontier molecular orbitals (FMOs) not only enhances Py-Cz-BN's CT properties but also creates a spatial site-blocking effect on the peripheral ^{t}Cz, thus further expanding the intermolecular distance between Py-BN cores. As illustrated in Fig. S6,† Py-Cz-BN has a shallower HOMO of 4.84 eV (5.18 eV for Py-BN) and LUMO of 1.83 eV (1.95 eV for Py-BN), respectively, and thus a narrower E_g of 3.01 eV (3.23 eV for Py-BN). Benefiting from the small reorganization energy (0.23 eV), the simulated spectrum of Py-Cz-BN shows a narrow FWHM of 0.12 eV/28 nm, and the main modes involved in the spectral progression are three twisting vibrations of 17.55–88.71 cm^{-1} and two stretching/scissoring vibrations of 290.0–443.2 cm^{-1} (Fig. S8 and S9†).

Photophysical characterization

Table 1 presents the photophysical properties of Py-Cz-BN, including the UV/Vis absorption and fluorescence spectra recorded in dilute toluene solution (1×10^{-5} M) and a 1 wt% doped film. Py-Cz-BN displays a sharp absorption band at a wavelength of 547 nm, which corresponds to the unique short-range charge transfer (SR-CT) transition (Fig. 5a). Due to its special *para* B–π–A structure, Py-Cz-BN emits a bright orange-red light with a peak at 586 nm and a small FWHM of 0.14 eV (40 nm). This represents a significant redshift of more than 37 nm compared to the benzene-centered BBCz-Y (which has an emission maximum of 549 nm and a FWHM of 0.17 eV/42 nm) (Fig. S11†). A small Stokes shift of 0.12 eV (37 nm) can be achieved, indicating a small structural displacement between the S_0 (ground state) and S_1 (excited state) of Py-Cz-BN.

Solvatochromic effect experiments were also performed. Fig. S12† shows that changing the solvents from weak (*n*-hexane) to strong (*N*,*N*-dimethylformamide) only caused a bathochromic shift of 18 nm in the emission spectra of Py-Cz-BN, demonstrating its singlet SRCT characteristic. The photoluminescence quantum yield (PLQY) was also measured to be as high as 99.2% under deoxygenated conditions. The calculated triplet state energy (T_1) from the 77 K phosphorescence spectrum (toluene solution) was 1.93 eV, resulting in a small S_1–T_1 energy difference (ΔE_{ST}) of 0.19 eV. This small value facilitates the reverse intersystem crossover (RISC) under ambient conditions. It should be noted that the presence of intramolecular hydrogen bonds in Py-Cz-BN reduces the dihedral angles between the central pyridine ring and the two peripheral carbazole units. This produces a relatively larger ΔE_{ST} and significantly increases the luminescence efficiency of the molecule (99.2%), which is undoubtedly

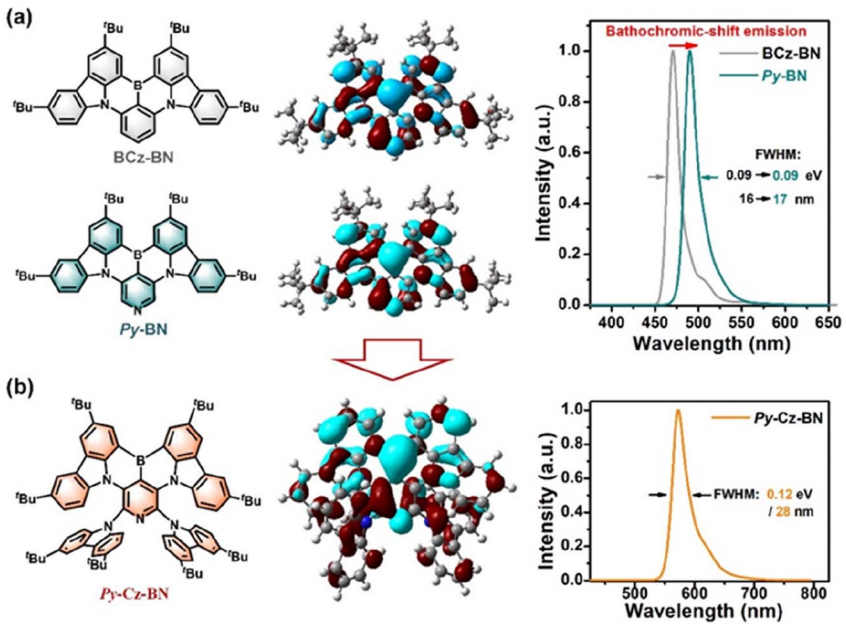

Fig. 4 Molecular structure (left), HOMO (one electron) and LUMO (one electron) distributions in the S_0 state (middle), and simulated vibrationally resolved fluorescence spectra with the dipole strengths of different vibrational modes (right) for BCz-BN (a, top), Py-BN (a, bottom) and Py-Cz-BN (b). Band broadening simulated by means of Gaussian functions with half-widths at half-maximum of 300.0 cm^{-1}.

Table 1 Summary of the photophysical data of Py-Cz-BN

	λ_{abs}[a] [nm]	λ_{PL}[a] [nm]	ΔE_{ST}[a] [eV]	FWHM[a] [eV]	FWHM[a] [nm]	τ_{PF}[b] (ns)	τ_{PF}[b] (μs)	HOMO[c]/LUMO[d] (eV)	PLQY[b]	k_r[b] (10^8 s^{-1})	k_{RISC}[b] (10^3 s^{-1})
Py-Cz-BN	547	586	0.19	0.14	40	3.8	739.0	4.82/-2.68	98.8%	2.4	1.5

[a] Measured in the toluene solution with a concentration of 10^{-5} mol L^{-1} (N_2). [b] Measured in mCBP: 1 wt% Py-Cz-BN doped film. [c] Measured in dry dichloromethane with a concentration of 10^{-3} mol L^{-1}. [d] Deduced from HOMO and energy gap (E_g) values.

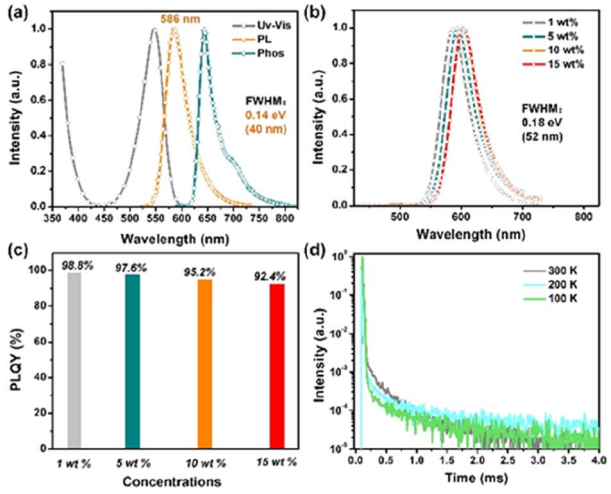

Fig. 5 (a) Ultraviolet/visible (UV/Vis) absorption, fluorescence (298 K), and phosphorescence (77 K) spectra of Py-Cz-BN in toluene (10^{-5} M). (b) The emission spectra of the doped films with different dopant concentrations in mCBP: *x* wt% Py-Cz-BN (*x* = 1, 5, 10, 15). (c) The PLQY values of the doped films with different dopant concentrations in mCBP: *x* wt% Py-Cz-BN (*x* = 1, 5, 10, 15). (d) Temperature-dependent transient PL decays of mCBP: 1 wt% Py-Cz-BN.

more important for MR emitters compared to the benzene-centered BBCz-Y (ΔE_{ST}: 0.14 eV and PLQY: 85%).

The photophysical properties of Py-Cz-BN in doped films (1, 5, 10, and 15 wt% doped mCBP, 3,3-bis(*N*-carbazolyl)-1,1′-biphenyl) were also measured to demonstrate the advantage of the sterically wrapped Py-MR-TADF (Fig. 5b–d and S13, S14†). As shown in Fig. 5b and c, unlike the conventional MR-TADF behaviors, concentration-induced radiation quenching and spectral broadening are well suppressed in Py-Cz-BN films, with consistently small FWHMs (0.18 eV/52 nm) and high PLQYs (92.4–98.8%) over a wide concentration range of 1–15 wt%. The relatively broader spectra could be assigned to the π–π interaction between the dopant and host material as well as the conformational change, which is a common phenomenon in MR-TADF systems.[1b] A temperature-dependent transient PL decay test confirmed the TADF nature of Py-Cz-BN, with a short-lived transient lifetime (τ_{PF}) of 3.8 ns and a long-lived delayed lifetime (τ_{DF}) of 739.0 μs in a 1 wt% doped film at room temperature (Fig. 5d). Combined with the high PLQY value of 98.8% at this concentration, the rate constants for the radiative decay (k_r) and RISC (k_{RISC}) of the molecule can be estimated to be 2.4×10^8 s^{-1} and 1.5×10^3 s^{-1}, respectively.[12] Efficient fluorescence and inefficient RISC processes are common manifestations of MR-TADF emitters. Additionally, the lifetime of the delayed component remains relatively constant with increasing doping concentration in Py-Cz-BN, indicating minimal molecular aggregation within this concentration range (Fig. S14†).

OLED device performances

Owing to the excellent photophysical properties, OLEDs employing Py-Cz-BN as the emitter were then fabricated with the structure of ITO/HATCN (1,4,5,8,9,11-hexaazatriphenylene hexacarbonitrile, 10 nm)/NPB (4,4′-*N*,*N*′-bis[*N*-(1-naphthyl)-*N*-phenylamino]biphenyl, 30 nm)/BCzPh (9,9′-diphenyl-9*H*,9′*H*-3,3′-bicarbazole, 10 nm)/mCBP: 20 wt% PO-01: *x* wt% Py-Cz-BN (*x* = 1, 5, 10, 15) (30 nm)/CzPhPy (4,6-bis(3-(9*H*-carbazol-9-yl)phenyl)′/pyrimidine, 10 nm)/DPPyA (9,10-bis(6-phenylpyridin-3-yl) anthracene, 30 nm)/LiF (0.5 nm)/Al (150 nm), where PO-01(Bis(4-phenyl-thieno[3,2-*c*]pyridinato-C2,*N*) (acetylacetonato)iridium(III)) was used as the phosphorescence sensitizer to assist the exciton recycle under electrical excitation.[13] As illustrated in Fig. S15,† significant absorption-emission spectral overlap and a large Förster energy transfer (FET) radius of 3.80 Å between the MR emitter and phosphorescence sensitizer could be obtained, suggesting efficient FET from PO-01 to Py-Cz-BN.[14] The energy level structure and electroluminescence behaviors of the adopted devices are shown in Fig. 6, S15–S19 and Table S1.† All devices exhibit orange-red emissions with peaks at 586–597 nm and small FWHMs of 0.18 eV (54 nm) that are nearly identical (Fig. 6b). The corresponding CIE coordinates range from (0.55, 0.45) to (0.60, 0.40), which are the ideal colors demanded in areas such as automotive taillights. The EQE_{max}–dopant concentration relationships are shown in Fig. 6c. High EQE_{max}s of 25.3–29.6% were recorded with the dopant concentration in the range of 1–15 wt%, which originated not only from the high PLQYs but also from the strong tendency to the horizontal dipole orientations (*Θ*//s: 75.5–82.0%) within the doped films (Fig. 6d and S18†). Notably, the EL operational stability is evaluated under an initial luminance of 5000 cd m^{-2} to give a long T90 lifetime (time to lose 10% of the initial luminance) of 152 h for the 1 wt% doped device, which is one of the best reported lifetimes for orange-red MR-OLEDs (Fig. S19†).[6h,15] The introduction of the pyridine acceptor could enhance the bond dissociation energy of the material in the anionic state, thus improving the operational stability of the Py-Cz-BN device.[16] Additionally, the transient EL decay curve showed a dominant fast decay, which also benefits a long operation lifetime by suppressing the residence time of the molecules in the excited states (Fig. S20†). The results demonstrate the significant role of the pyridine-centered

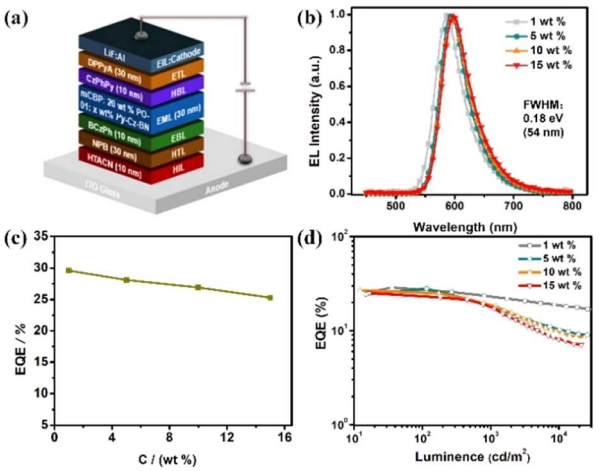

Fig. 6 (a) Device structure. (b) The EL spectra of the Py-Cz-BN devices recorded at 1000 cd m^{-2}. (c) The EQE_{max}–dopant concentration relationship in Py-Cz-BN based OLEDs. (d) The EQE–luminance curves of the Py-Cz-BN devices.

skeleton in constructing long-wavelength MR-TADF emitters. It is expected that this strategy will lead to further breakthroughs in narrowband materials and devices.

Conclusions

In summary, we have synthesized the first pyridinyl-centered MR-TADF emitter, named Py-Cz-BN, successfully, by introducing site-resistive substituents. The text describes the possible reaction mechanisms in detail, with the help of electrostatic potential (ESP) calculations and others. Changing the MR center from phenyl to pyridine enhanced the charge transfer properties and structural rigidity of the target molecule. This resulted in a significantly bathochromically shifted emission of more than 37 nm and a 0.03 eV reduction in the FWHM. Py-Cz-BN displays a bright orange-red emission with an emission wavelength of 586 nm, a small FWHM of 0.14 eV (40 nm), and a high PLQY of 99.2% in dilute toluene solution. Featuring a special bilaterally shielded structure of Py-Cz-BN, the optimized OLEDs exhibited high EQE_{max}s of 25.3–29.6% and nearly identical small FWHMs of 0.18 eV (54 nm) over a wide doping range of 1–15 wt%. Additionally, an impressive long LT90 lifetime of 152 hours was also recorded at an initial brightness of 5000 cd m^{-2}. We believe that this reaction mechanism and design strategy will greatly enrich the structural diversity of B,N-based MR skeletons and accelerate the development of high-performance narrowband emitters and OLEDs.

Data availability

The data are available from the corresponding author on reasonable request.

Author contributions

M. Du carried out most parts of the experiments and wrote the original manuscript. M. Mai contributed to the DFT calculations. D. Zhang and L. Duan supervised the project and analysed the data and they provided comments and revised the whole work with Y. Zhang.

Conflicts of interest

There are no conflicts to declare.

Acknowledgements

This work was supported by the Young Scientists Fund of the (http://ir.ipe.ac.cn/handle/122111/39931) NSFC (Grant No. 52203230), the National Key Research and Development Program (Grant No. 2022YFA1204404, 2023YFE0203300, 2022YFB3603002, and 2021YFB3602702), the National Natural Science Foundation of China (Grant No. 22135004, 51903137, and 61890942) http://ir.ipe.ac.cn/handle/122111/39931, and the Young Elite Scientists Sponsorship Program by CAST (Grant No. 2022QNRC001) and China Postdoctoral Science Foundation (Grant No. 043260519).

Notes and references

1 (*a*) F. Santoro, A. Lami, R. Improta, J. Bloino and V. Barone, *J. Chem. Phys.*, 2008, **128**, 224311; (*b*) Y. Kondo, K. Yoshiura, S. Kitera, H. Nishi, S. Oda, H. Gotoh, Y. Sasada, M. Yanai and T. Hatakeyama, *Nat. Photonics*, 2019, **13**, 678–682.

2 (*a*) J. M. Ha, S. H. Hur, A. Pathak, J.-E. Jeong and H. Y. Woo, *NPG Asia Mater.*, 2021, **13**, 53; (*b*) G. V. Baryshnikov, D. A. Sunchugashev, R. R. Valiev, B. F. Minaev and H. Ågrenad, *Chem. Phys.*, 2018, **513**, 105–111.

3 (*a*) T. Hatakeyama, K. Shiren, K. Nakajima, S. Nomura, S. Nakatsuka, K. Kinoshita, J. Ni, Y. Ono and T. Ikuta, *Adv. Mater.*, 2016, **28**, 2777–2781; (*b*) Y. Zhang, D. Zhang, J. Wei, X. Hong, Y. Lu, D. Hu, G. Li, Z. Liu, Y. Chen and L. Duan, *Angew. Chem., Int. Ed.*, 2020, **59**, 17499; (*c*) Y. Zhang, J. Wei, D. Zhang, C. Yin, G. Li, Z. Liu, X. Jia, J. Qiao and L. Duan, *Angew. Chem., Int. Ed.*, 2022, **61**, e202113206; (*d*) Y. Zhang, G. Li, L. Wang, T. Huang, J. Wei, G. Meng, X. Wang, X. Zeng, D. Zhang and L. Duan, *Angew. Chem., Int. Ed.*, 2022, **61**, e202202380; (*e*) X. F. Luo, S. Q. Song, H. X. Ni, H. Ma, D. Yang, D. Ma, Y. X. Zheng and J. L. Zuo, *Angew. Chem., Int. Ed.*, 2022, **61**, e202209984; (*f*) Y. Xu, C. Li, Z. Li, Q. Wang, X. Cai, J. Wei and Y. Wang, *Angew. Chem., Int. Ed.*, 2020, **59**, 17442; (*g*) X. G. Wu, B. K. Su, D. G. Chen, D. H. Liu, C. C. Wu, Z. X. Huang, T. C. Lin, C. H. Wu, M. B. Zhu, E. Y. Li, W. Y. Hung, W. G. Zhu and P. T. Chou, *Nat. Photonics*, 2021, **15**, 780; (*h*) Y. Zou, M. Yu, J. Miao, T. Huang, S. Liao, X. Cao and C. Yang, *Chem. Sci.*, 2023, **14**, 3326; (*i*) X.-C. Fan, K. Wang, Y.-Z. Shi, Y.-C. Cheng, Y.-T. Lee, J. Yu, X.-K. Chen, C. Adachi and X.-H. Zhang, *Nat. Photonics*, 2023, **17**, 280–285; (*j*) M. Yang, I. S. Park and T. Yasuda, *J. Am. Chem. Soc.*, 2020, **142**, 19468–19472; (*k*) S. M. Suresh, D. Hall, D. Beljonne, Y. Olivier and E. Z. Colman, *Adv. Funct. Mater.*, 2020, **30**, 1908677; (*l*) J. Bian, S. Chen, L. Qiu, R. Tian, Y. Man, Y. Wang, S. Chen, J. Zhang, C. Duan, C. Han and H. Xu, *Adv. Mater.*, 2022, **34**,

2110547; (*m*) Y. Liu, X. Xiao, Z. Huang, D. Yang, D. Ma, J. Liu and J. You, *Angew. Chem., Int. Ed.*, 2022, **61**, e202210210; (*n*) F. Liu, Z. Cheng, Y. Jiang, L. Gao, H. Liu, H. Liu, Z. Feng, P. Lu and W. Yang, *Angew. Chem., Int. Ed.*, 2022, **61**, e202116927; (*o*) Y.-K. Qu, D.-Y. Zhou, F.-C. Kong, Q. Zheng, X. Tang, Y.-H. Zhu, C.-C. Huang, Z.-Q. Feng, J. Fan, C. Adachi, L.-S. Liao and Z.-Q. Jiang, *Angew. Chem., Int. Ed.*, 2022, **61**, e202201886.

4 (*a*) X. Wang, L. Wang, G. Meng, X. Zeng, D. Zhang and L. Duan, *Sci. Adv.*, 2023, **9**, eadh143; (*b*) X. Lv, J. Miao, M. Liu, Q. Peng, C. Zhong, Y. Hu, X. Cao, H. Wu, Y. Yang, C. Zhou, J. Ma, Y. Zou and C. Yang, *Angew. Chem., Int. Ed.*, 2022, **61**, e202201588; (*c*) K. Rayappa Naveen, H. Lee, R. Braveenth, K. Joon Yang, S. Jae Hwang and J. Hyuk Kwon, *Chem. Eng. J.*, 2022, **432**, 134381.

5 (*a*) M. Yang, S. Shikita, H. Min, I. S. Park, H. Shibata, N. Amanokura and T. Yasuda, *Angew. Chem., Int. Ed.*, 2021, **60**, 23142–23147; (*b*) J. Liu, Y. Zhu, T. Tsuboi, C. Deng, W. Lou, D. Wang, T. Liu and Q. Zhang, *Nat. Commun.*, 2022, **13**, 4876.

6 (*a*) Y. Zhang, D. Zhang, T. Huang, A. J. Gillett, Y. Liu, D. Hu, L. Cui, Z. Bin, G. Li, J. Wei and L. Duan, *Angew. Chem., Int. Ed.*, 2021, **60**, 20498; (*b*) Y. Liu, X. Xiao, Y. Ran, Z. Bin and J. You, *Chem. Sci.*, 2021, **12**, 9408; (*c*) Y. Zou, J. Hu, M. Yu, J. Miao, Z. Xie, Y. Qiu, X. Cao and C. Yang, *Adv. Mater.*, 2022, **34**, 2201442; (*d*) X. Cai, Y. Xu, Y. Pan, L. Li, Y. Pu, X. Zhuang, C. Li and Y. Wang, *Angew. Chem., Int. Ed.*, 2023, **62**, e202216473; (*e*) H. Chen, T. Fan, G. Zhao, D. Zhang, G. Li, W. Jiang, L. Duan and Y. Zhang, *Angew. Chem., Int. Ed.*, 2023, **62**, e202300934; (*f*) T. Fan, M. Du, X. Jia, L. Wang, Z. Yin, Y. Shu, Y. Zhang, J. Wei, D. Zhang and L. Duan, *Adv. Mater.*, 2023, **35**, 2301018; (*g*) K. R. Naveen, S. J. Hwang, H. Lee and J. Hyuk Kwon, *Adv. Electron. Mater.*, 2022, **8**, 2101114; (*h*) X.-C. Fan, F. Huang, H. Wu, H. Wang, Y.-C. Cheng, J. Yu, K. Wang and X.-H. Zhang, *Angew. Chem., Int. Ed.*, 2023, **62**, e2023055.

7 (*a*) Y. Xiang, P. Li, S. Gong, Y.-H. Huang, C.-Y. Wang, C. Zhong, W. Zeng, Z. Chen, W.-K. Lee, X. Yin, C.-C. Wu and C. Yang, *Sci. Adv.*, 2020, **6**, eaba7855; (*b*) P. Rajamalli, N. Senthilkumar, P.-Y. Huang, C.-C. Ren-Wu, H.-W. Lin and C.-H. Cheng, *J. Am. Chem. Soc.*, 2017, **139**, 10948–10951; (*c*) Y. He, Z. Qiao, X. Cai, M. Li, W. Li, W. Xie, W. Qiu, L. Wang and S.-J. Su, *ACS Appl. Mater. Interfaces*, 2020, **12**, 49905–49914.

8 Y. Zhang, D. Zhang, J. Wei, Z. Liu, Y. Lu and L. Duan, *Angew. Chem., Int. Ed.*, 2019, **58**, 16912–16917.

9 C. Chen, C.-Z. Du and X.-Y. Wang, *Adv. Sci.*, 2022, **9**, 2200707.

10 (*a*) Z. G. Zhou, A. Wakamiya, T. Kushida and S. Yamaguchi, *J. Am. Chem. Soc.*, 2012, **134**, 4529; (*b*) S. Saito, K. Matsuo and S. Yamaguchi, *J. Am. Chem. Soc.*, 2012, **134**, 9130; (*c*) T. Kushida, C. Camacho, A. Shuto, S. Irle, M. Muramatsu, T. Katayama, S. Ito, Y. Nagasawa, H. Miyasaka, E. Sakuda, N. Kitamura, Z. Zhou, A. Wakamiya and S. Yamaguchi, *Chem. Sci.*, 2014, **5**, 1296.

11 L. Zhou and G. Zhang, *Angew. Chem., Int. Ed.*, 2020, **59**, 8963–8968.

12 Y. Wada, H. Nakagawa, S. Matsumoto, Y. Wakisaka and H. Kaji, *Nat. Photonics*, 2020, **14**, 643–649.

13 D. R. Lee, J. Lim and J. Y. Lee, *Org. Electron.*, 2021, **94**, 106166.

14 B. W. D'Andrade, M. A. Baldo, C. Adachi, J. Brooks, M. E. Thompson and S. R. Forrest, *Appl. Phys. Lett.*, 2001, **79**, 1045–1047.

15 G. Meng, H. Dai, J. Zhou, T. Huang, X. Zeng, Q. Wang, X. Wang, Y. Zhang, T. Fan, D. Yang, D. Ma, D. Zhang and L. Duan, *Chem. Sci.*, 2023, **14**, 979–986.

16 R. Wang, Q.-Y. Meng, Y.-L. Wang and J. Qiao, *CCS Chem.*, 2022, **4**, 331–343.